# Coherent Control of Two-Photon-Induced Photocurrents in Semiconductors With Frequency-Dependent Response

Jung-Ho Chung, *Member, IEEE*, and Andrew M. Weiner, *Fellow, IEEE*

***Abstract*—In this paper, two-photon (TP)-induced photocurrents in two different semiconductor diodes were coherently controlled simultaneously via phase-only shaping of femtosecond pulses. Because of their distinct TP absorption (TPA) spectral responses, the diodes generated noticeably different photocurrent yields depending on the pulse shape. By adjusting second- and third-order dispersion coefficients, we demonstrated that the yield contrast is enhanced when excited by the pulse, whose second-harmonic (SH) spectrum has a peak around the spectral range where those TPA spectral responses differ widely. Also, the photocurrent yield ratio was maximized or minimized using an optimization algorithm, with extremes corresponding to 1.20 and 0.75, respectively. Finally, it was demonstrated that different traces can result when autocorrelation (AC) functions of identical pulses are measured by those diodes with distinct TPA spectral responses.**

***Index Terms*—Coherent control, pulse shaping, two-photon absorption (TPA), ultrafast optics.**

## I. Introduction

FOR a decade or more, coherent control schemes for laser control over electronic, atomic, or molecular behaviors have been explored in physics and chemistry [1]. Such schemes are generally based on quantum interference among multiple excitation pathways [2]. One can maximize or minimize desired process outcomes through constructive or destructive interferences of such pathways, usually by manipulation of phase. In early experiments, e.g., [3] and [4], only the interval between two successive pump pulses or the relative phase between fundamental and second-harmonic (SH) pulses could be adjusted. By using femtosecond pulse-shaping technology [5], however, almost any desired waveforms can be obtained; this has been one of the main factors enabling many significant results in recent coherent control research [6]–[10]. Demonstrations include turning on or off the nonresonant two-photon (TP) transition in cesium [6], selectively breaking chemical bonds in molecules to optimize the ratio of the resulting chemical products [7], [8], and controlling second-harmonic generation (SHG) for spectral phase characterization [9] and for use in selective TP excitation of a pH-sensitive chromophore [10]. A detailed discussion of various control objectives, target materials, and so on can be found in previous review papers, [1] or [2].

In contrast to such coherent control experiments in atomic or molecular systems, in this paper we focus on coherent control in semiconductors, in particular, coherent control of their TP absorption (TPA). In the long run, semiconductor-based coherent control has the potential to evolve into practical applications due to mature semiconductor manufacturing technologies. Previous work on coherent control in semiconductors has dealt with inhomogeneous broadening effects [11], terahertz emission and carrier populations in heterostructures [12], photogenerated excitons in quantum wells [3], the direction of electrical currents in a AlGaA–GaAs quantum well [4] or in a GaAs bulk crystal [13], TP transitions [14], phonon effects [15], and biexcitonic polarization [16] in multiple quantum wells (MQWs), differential transmission in AlGaAs [17], biexcitonic states in a quantum dot [18], TPA in CdS and GaAsP for the purpose of pulse compression [19], free-carrier density in GaAs [20], manipulation of Bloch oscillations in superlattices [21], and so on. In [14], the TP photoluminescence have been analyzed as a function of delay between a signal-reference pulse pair, while in [19] TP-induced photocurrents in semiconductors have been used as a diagnostic for chirp compensation and pulse compression using spectral phase pulse shaping.

To date, only few semiconductor-based experiments have exploited the capabilities of programmable pulse-shaping technology for coherent control of TP-induced photocurrents. Moreover, real-time manipulation of the ratio of two different coherent control output variables, such as control of product ratios in the case of selective bond breaking in molecules [7], [8], has not yet been reported in all semiconductor systems. In this paper, we demonstrate, for the first time to our knowledge, coherent control of the ratio of TP-induced photocurrents generated simultaneously in two different semiconductor devices. Very recently, a similar experiment was reported, with the difference that TP excitation of a semiconductor was compared with TP excitation in dye materials [22]. The basis of our experiments is the frequency dependence of the TP response, which can be different in different semiconductor devices. This enables manipulation of the TP photocurrent ratios under pulse shape control. Generally, a stronger degree of coherent control is expected for more widely differing TPA spectral responses and for wider bandwidths. Nevertheless, in this paper we successfully demonstrate coherent control results even though we are using commercial devices as TP detectors (which afford little opportunity for designing the TP spectral responses)

Manuscript received October 31, 2005; revised January 30, 2006. This work was supported by the National Science Foundation under Grant 0210445-ECS.

J.-H. Chung was with Purdue University, West Lafayette, IN 47907 USA. He is now with Massachusetts Institute of Technology, Cambridge, MA 02139 USA (e-mail: chungj@mit.edu).

A. M. Weiner is with the School of Electrical and Computer Engineering, Purdue University, West Lafayette, IN 47907 USA (e-mail: amw@ecn.purdue.edu).

Digital Object Identifier 10.1109/JSTQE.2006.872043

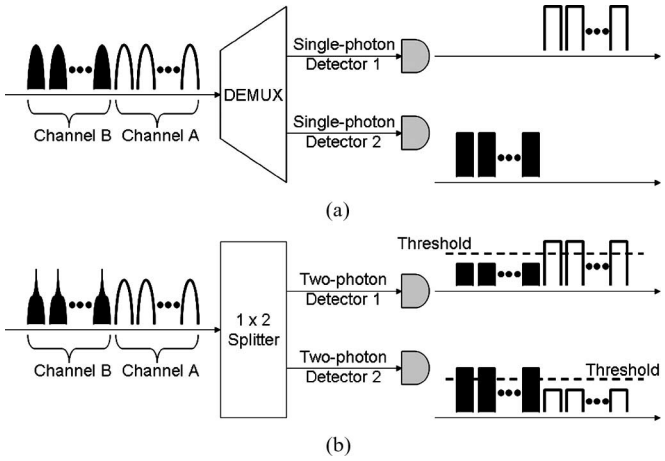


Fig. 1. Demultiplexer-free detection scheme. (a) Conventional single-photon detection of time-division multiplexed signals and (b) newly proposed TP detection of chirp-coded signals. DEMUX: demultiplexer.

and relatively long, $\sim$150 fs pulses with small fractional bandwidth.

As briefly mentioned above, coherent control in semiconductors is important due to its potential for real-world applications. For example, interference phenomena associated with photogenerated wave packets in heterostructures have been proposed for future terahertz-regime high-speed switching devices [23]. Femtosecond-order optical switching using coherent destruction of photogenerated excitons in MQWs has also been proposed [3]. In this paper, we propose a new application perspective that could potentially be enabled by our semiconductor coherent control approach.

Let us assume that two semiconductor diodes are specially designed so that pulse shape A generates a time-integrated TP-induced photocurrent that is above a certain threshold in diode 1, while the photocurrent in diode 2 remains below the threshold. We assume that pulse shape B is designed to do the converse: the photocurrent it induces is above threshold in diode 2, but not in diode 1. We further consider the case of on–off keyed optical data in a slotted optical time-division multiplexed (OTDM) network, with bits corresponding to channels A and B transmitted as pulse shapes A and B, respectively. Conventionally, a demultiplexer performing a time-domain switching operation is required to separate the channels, which are then detected by a single-photon photodetector, as illustrated in Fig. 1(a). In this case the optical phase is neglected. In contrast, in our scheme a $1 \times 2$ splitter couples the data stream onto the two TP diodes, which detect their respective matched pulse shapes in parallel. Thus, diode 1 selectively detects bits composed of pulse shape A, since its response to bits composed of shape B falls below the threshold, whereas diode 2 detects only channel B [see Fig.1(b)]. Note that single-photon detectors cannot discriminate between the channels in this case, assuming that the waveforms are of equal energy and distinguishing temporal features are faster than the data rate limited by photodiode response. This demultiplexer-free detection scheme can be extended to the N-channel case, as long as there is enough optical power to allow power splitting to $N$ distinct TP detectors and the contrast in the TP spectral responses is sufficient.

An interesting alternative scheme would be to use a diode with TPA spectral response that varies with bias. If the degree of variation is sufficient, we may be able to find a set of optimum pulse shapes, each of which generates a TPA yield above the threshold at a specific bias voltage but not at other voltages. Properly structured MQW diodes are known to show TPA responses that red-shift with bias [24]–[26]. In addition, many attempts have been made to impart wavelength tunability to (single-photon) semiconductor detectors [27]–[37]; some of these ideas may be applicable to our TP scheme. Note also that in single-channel data transmission, we can envision pulse-shape keying in place of on–off keying, i.e., pulse shapes A and B represent bits 1 and 0, respectively. In this case diode 1 receives correct data stream but diode 2 detects inverted bits. This kind of transmission may be advantageous from the point of view of security, since without knowing the waveforms or the TPA spectral responses, it will be difficult for an eavesdropper to determine the data. This idea is similar to recent work in optical code division multiple access (O-CDMA), where a code switching data modulation scheme gives some degree of increased eavesdropping resistance compared to on–off keying [38], [39].

Our investigation is also relevant to TPA-based pulsewidth measurements. TPA in laser diodes (LDs), photodiodes (PDs), or even light-emitting diodes (LEDs) has been often used for autocorrelation (AC) measurements as an alternative to SHG (for example, [40]–[43]). TPA is widely believed to circumvent problems such as finite phase-matching bandwidth and group velocity mismatch that are inherent in the SHG measurement. However, several requirements should be satisfied to perform TPA-based pulsewidth measurements. First, the incident optical power should fall in the regime where the generated photocurrent is quadratic in the input peak power. Second, assuming a fixed pulse shape, the photocurrent should be inversely proportional to the pulsewidth [44]. Third (closely related to the second condition), the TPA spectral response should be flat. Otherwise, the spectral response may introduce effects similar to those that occur in SHG with limited phase-matching bandwidth, which would introduce errors in the correlation measurement [45]. This third aspect, however, has been seldom examined in previous pulsewidth measurements, even though the TPA spectral response of GaAsP was measured in [41]. It has been believed that for shorter pulsewidths the TPA-based measurement is preferable, since SHG is more subject to the finite phase-matching bandwidth. One should remember, however, that for shorter pulses, a nonflat TPA spectral response also plays a more significant role. Therefore, it is worthwhile to discuss how the TPA spectral response in semiconductor diodes modifies measured AC traces. To do this, we compared the AC traces acquired using diodes with distinct TPA spectral responses. We observed that depending on pulse shapes, traces measured with one diode can be either wider or shorter than those with the other diode. We have also observed correlation between coherently controlled TP photocurrent yields in different diodes and the relative AC widths returned using those diodes.

This paper is organized as follows: In Section II, a brief theory related to TPA and the experimental setup will be discussed and the spectral response measurements will be also explained. Coherent control experiments and AC measurements will be covered in Sections III and IV, respectively. Finally, in Section V we present conclusion.

## II. Brief TPA Principle and Experiment Overview

### A. TPA Principle

When an ultrashort pulse $e(t)$ oscillating with an angular frequency of $\omega_0$ nonresonantly interacts with a two-level system, the probability of the TP transition can be written approximately as [6]

$$S_2 = \int_{-\infty}^{\infty} H(\omega) \left| \int_{-\infty}^{\infty} e^2(t) \exp(-j\omega t)\, dt \right|^2 d\omega \qquad (1)$$

where $\omega$ represents the angular frequency and $H(\omega)$ is the TPA spectral response function. The remaining factor in the integrand represents the SH spectrum induced by the excitation pulse and can be written as $|F_t\{e^2(t)\}|^2$, where $F_t\{\cdot\}$ represents the Fourier transform with respect to $t$. Note that the SH spectrum is centered around the resonance frequency $\omega_r$ approximately equal to $2\omega_0$. This transition can be observed from TP fluorescence, photocurrent, etc. Since this formula corresponds to TPA without any intermediate resonances, the TPA response is expected to depend only on the final TP energy. In [6], high contrast coherent control of TP fluorescence was demonstrated in an atomic vapor, which is in the narrow TP linewidth limit. Note that (1) also describes the SHG yield in the case of a narrow phase-matching bandwidth. Through this analogy it has also been demonstrated that by using pulse shaping, the SHG yield can be coherently controlled with over three orders of magnitude contrast [46]. In the opposite limit where $H(\omega)$ has a very wide linewidth [i.e., when $H(\omega)$ is a flat continuum], (1) reduces to $S_2 = \int I^2(t)dt$, where $I(t) = |e(t)|^2$, which is desirable for pulsewidth measurements [40]–[44]. Note that in this limit, there is no dependence on the temporal phase so that coherent control is not possible.

In general, the TP spectral response is neither narrow nor completely frequency independent. On the one hand, this can lead to errors in interpreting AC traces acquired using TP devices. On the other hand, frequency-dependent TP response allows coherent control for manipulation of the relative photocurrent yields in TP detectors with distinct spectral responses $H_1(\omega)$ and $H_2(\omega)$.

### B. Experiment Overview

We performed TP experiments using input light in the 1.5-$\mu$m band and two commercially available diodes, a surface-normal PIN silicon (Si) PD (Thorlabs PDA55) and a 784-nm edge-emitting LD (Sharp GH0781JA2C). The latter is believed to have AlGaAs–GaAs MQW structure. In principle, one may design diodes whose TPA spectral responses are optimized for strong spectral dependence (hence, large coherent control contrasts) by locating exciton peaks at desired TP wavelengths; however, in this paper, we show clear contrast even using commercial diodes. As commonly known, the Si PD has a fairly flat spectral response at the TP wavelength ($\sim$780 nm) since its band edge is far from the final TPA levels. In contrast, in the LD the final TPA states are located close to the band edge so that a strong spectral response may be introduced.

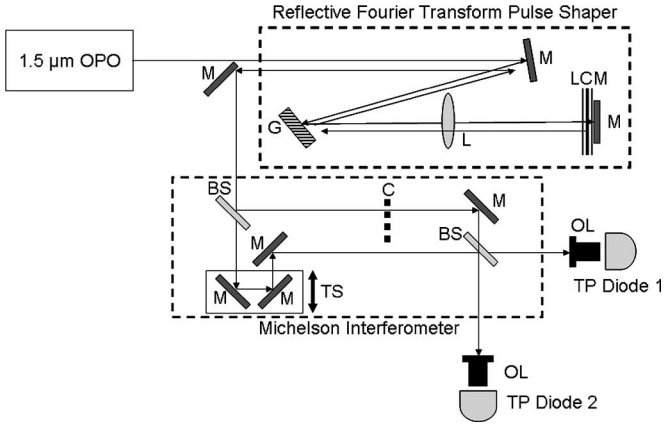


Fig. 2. Schematic of the experimental setup. OPO: optical parametric oscillator; M: mirror; G: grating; L: lens; LCM: liquid crystal modulator; BS: beam splitter; C: chopper; TS: translational stage; OL: objective lens; TP: two-photon.

The experimental setup is illustrated in Fig. 2. Femtosecond pulses with $\sim$15-nm bandwidth emitted from an optical parametric oscillator (OPO, Spectra Physics) were passed through a reflective Fourier transform pulse shaper [5], chopped, and then split into two arms for simultaneous coupling into the two diodes through $20\times$ microscope objective lenses. The diodes were uncapped to prevent unwanted multiple light reflections. Both diodes were unbiased and connected via respective 320-k$\Omega$ resistors to respective lockin amplifiers, where the photocurrents induced by TPA of the input pulses were measured. For each diode, the dependence of the photocurrent on the optical power was examined to identify the range of the quadratic regime. In all the following experiments, optical powers were adjusted so that they always resided within this quadratic regime. The Michelson Interferometer shown in the figure is not used in this stage of the experiments, but is used later when we explore the effect of TP spectral response on pulsewidth measurements.

The pulse shaper consisted of a grating with 830 grooves/mm, 200-mm lens, 2-layer 128-pixel liquid crystal modulator (LCM: 256-MIR, CRi) with 0.1-mm pixel width, and mirror. At the grating, incident and diffracted angles were 45° and 31°, respectively. At the LCM a spectral spread of 0.52 nm per pixel and a spectral resolution less than 2-pixel width were obtained. Only phase was modulated for coherent control via a computer programmable LCM controller (SLM-256, CRi). The dispersion due to the laser source, pulse shaper, or lenses was compensated by optimizing the grating-lens distance in the pulse shaper so that a shortest pulsewidth was measured through the AC acquired via TPA of the Si PD. Higher order dispersions turned out to be negligible when the spectral phase profile of the resultant pulse was examined by applying an evolutionary algorithm,

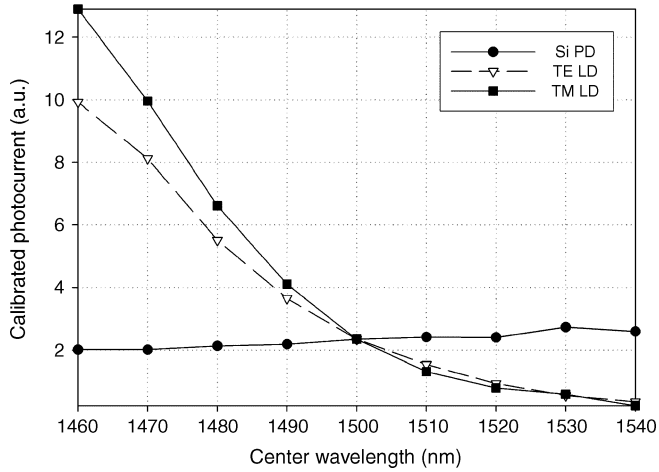


Fig. 3. TPA spectral responses obtained by calibrating TP-induced photocurrents in the Si PD (solid line with circles) and 784-nm LD for TE polarization (dashed line with triangles) and TM polarizations (solid line with squares) as functions of the center wavelength of the pulse with ∼15-nm bandwidth.

as in [19]. Details on the algorithm we used for optimization are given in Section III.

### C. Measurement of TPA Spectral Responses

TPA spectral response functions were investigated by measuring TP-induced photocurrent yields from the two diodes while adjusting the center wavelength of unshaped excitation pulses. The spectral resolution is limited by the pulse spectrum with a full-width at half-maximum (FWHM) of ∼15 nm. Optical powers were adjusted so that the two diodes had identical lockin amplifier readings at 1500 nm. Resulting photocurrents were calibrated by multiplying (pulsewidth), $(\text{power})^{-2}$, and $(\text{wavelength})^2$, as in [41]. While the former two factors reflect requirements for TPA-based pulsewidth measurement explained in Section I, the third factor accounts for varying focused spot sizes. Although it depends on the active area of a diode, the third factor was applied to both LD and PD cases since it introduced only minor changes in the calibration. In contrast to the silicon case, the LD responded differently depending on the beam polarization. Transverse-electric (TE)-polarized pulses gave better sensitivity while the wavelength dependence was somewhat stronger for transverse-magnetic (TM)-polarized pulses. This phenomenon is believed to result from polarization-dependent mode coupling and electron transition imposed by the device structure. Fig. 3 shows the calibrated photocurrent as a function of the OPO wavelength. While silicon has a fairly flat response, curves for the LD are monotonically decreasing with wavelength, indicating the typical band edge characteristic. The TM-case response of the LD is stronger than the TE case, as mentioned ealier. Note that they intersect with one another at 1500 nm, since their lockin amplifier outputs were made identical at this point. These curves directly tell what we can expect in the coherent control experiment using the pulse centered at 1500 nm. Also note that a high-resolution method using the Fourier transform of interferometric autocorrelation (IAC), proposed in [22], gave the result similar to Fig. 3.

## III. Coherent Control Experiments

TPA coherent control experiments in the foregoing semiconductors were possible due to their distinct spectral responses. Certain pulse shapes lead to the SH spectra that can be weighted more or less in one diode than the other, resulting in larger or smaller TPA yields, as explained mathematically in (1). In order to demonstrate coherent control of TPA, we used two different approaches for selecting the pulse shapes. Both approaches are discussed in this section.

### A. Adjustment of Second- and Third-Order Dispersion Coefficients

In this approach, we used the pulse shaper to apply spectral phase profiles consisting of second- and third-order dispersion coefficients. The coefficients were varied to generate different pulse shapes that led to different photocurrent contrasts. The Fourier transform of $e(t)$ in (1) can be written as $E(\omega) = A(\omega)\exp[j\psi(\omega)]$, where $A(\omega)$ is the amplitude, whose square gives the power spectrum, and $\psi(\omega)$ is the spectral phase. We shaped the pulse by changing the second- and third-order dispersion coefficients, $\beta_2$ and $\beta_3$, in

$$\psi(\omega) = \frac{\beta_2}{2}(\omega-\omega_0)^2 + \frac{\beta_3}{6}(\omega-\omega_0)^3 \tag{2}$$

while $A(\omega)$ was not modulated. For each diode, we produced a contour plot of the photocurrent, with each point's coordinate determined by $\beta_2$ and $\beta_3$ used for inducing it. These were then normalized so that the center of the plot, representing the transform-limited case, always has unity. Fig. 4(a) and (b) corresponds to contour plots of normalized TP-induced photocurrents in the LD for TM polarization and Si PD, respectively, when the excitation pulse spectrum is centered at 1476 nm. In order to produce these graphs, 21 points per axis were used, resulting in spacing of $\sim 0.031\ \text{ps}^2$ for $\beta_2$ and $\sim 0.0032\ \text{ps}^3$ for $\beta_3$. Compared to those in Fig. 4(b), contours in Fig. 4(a) are slightly rotated in a clockwise sense. This reflects different slopes of their TPA spectral responses, as shown in Fig. 3. Note that in the case of the ideally flat spectral response, these contours should be symmetric with respect to both axes. Minor asymmetric features in Fig. 4(b) are believed to reflect the slight nonflatness of the silicon response in Fig. 3. This slope is negligibly small so that its simulation results were almost identical to the ideal case. At each coordinate we calculated the ratio of the normalized photocurrent in Fig. 4(a) to that in Fig. 4(b). This is shown in Fig. 4(c). Maxima (brighter regions) and minima (darker regions) are distributed around upper left and lower right corners and around upper right and lower left corners, respectively. Maximum and minimum ratios were 1.03 and 0.74, respectively.

This distribution can be understood by examining the location of the SH spectrum peak, as shown in Fig. 4(d). The peak location was obtained by computer calculation using the measured power spectrum. Nearly nonchirped pulses have SH spectra centered at 738 nm. For the coefficients corresponding to upper-left and lower-right corners, however, SH spectra are centered at wavelengths less than 738 nm, where the LD response is stronger than silicon (see Fig. 3). According to (1),

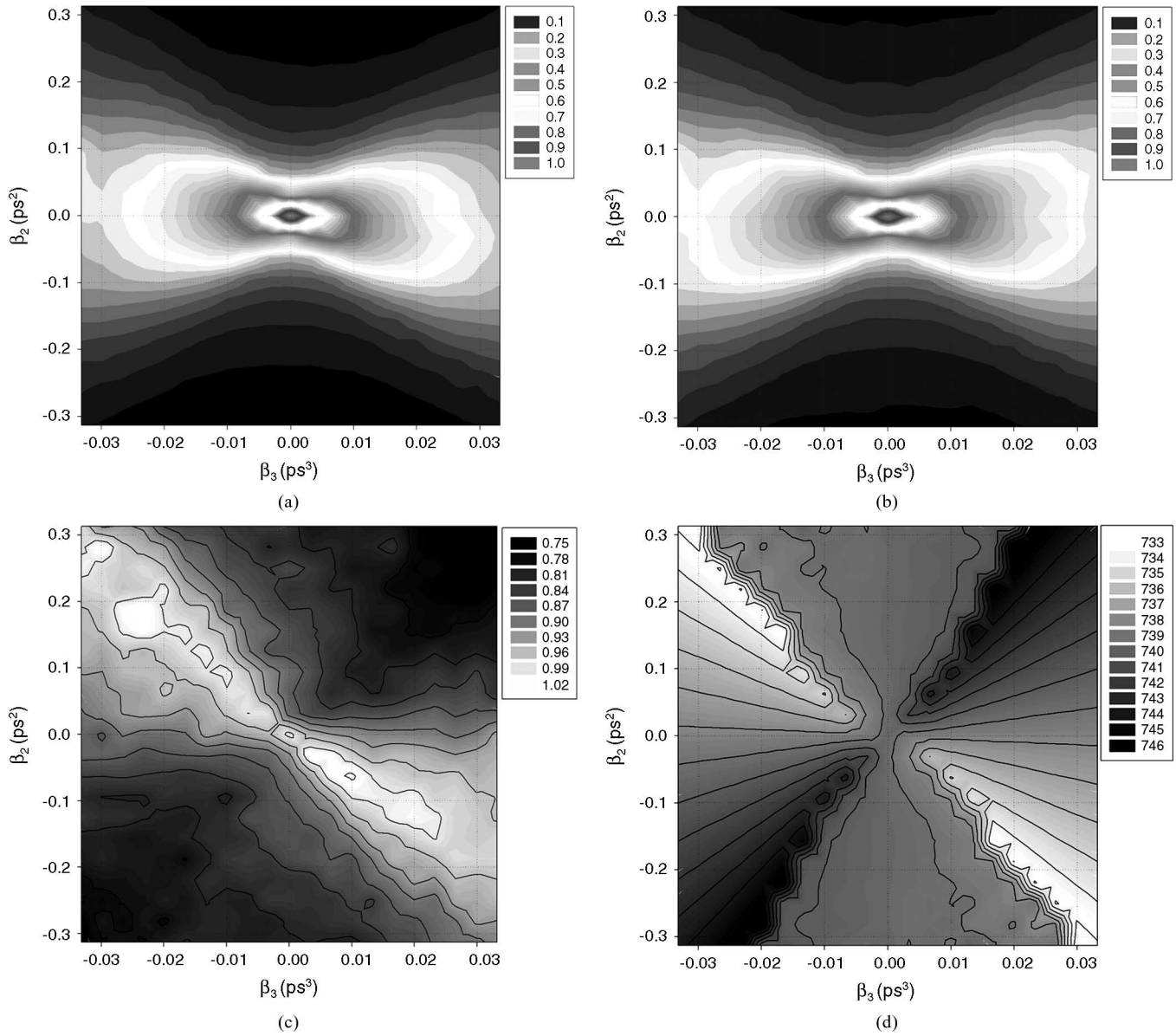


Fig. 4. Coherent control using second- and third-order chirp coefficients in cases with (a) the LD for TM polarization and (b) the Si PD, respectively. (c) Ratios of those in (a) to those in (b). (d) Simulated location of the SH spectrum peak.

the LD yielded larger photocurrents, as in Fig. 4(c). At other two corners, SH spectra have peaks at wavelengths longer than 738 nm, where the LD response is weaker than silicon, resulting in smaller yields in the LD.

### *B. Contrast Maximization Using an Evolutionary Algorithm*

To find the optimum pulse shapes that maximize the yield contrast, we utilized an evolutionary algorithm. In this algorithm, a set of parameters, dubbed an individual, evolves in a group through recombination, mutation, and selection for the survival of the fittest. Exhaustive discussions can be found in [48] and one of its applications on the semiconductor coherent control is reported in [17]. In our algorithm, the individual was the phase as a function of wavelength, consisting of an array of 64 elements (or so called genes). Each phase profile gave rise to a certain pulse shape and, with the measured power spectrum and TPA spectral responses, the corresponding photocurrent yields could be calculated using (1). The ratio of the two photocurrents normalized by the respective nonchirped case yields was used for the merit function, according to which best individuals were selected and used in recombination and mutation processes to generate next-generation individuals. These steps were repeated until the population of individuals grew almost identical. The resultant solutions were interpolated into 128 elements and applied to the LCM in the pulse shaper. The shaped pulse generated TP-induced photocurrents simultaneously in the two diodes, and photocurrents from respective lockin amplifiers were read by a computer. Here, the beam incident upon the Si PD was attenuated to compensate for the sensitivity mismatch.

Fig. 5(a) shows the spectral phase profile of the algorithm found to maximize the ratio of the normalized photocurrent

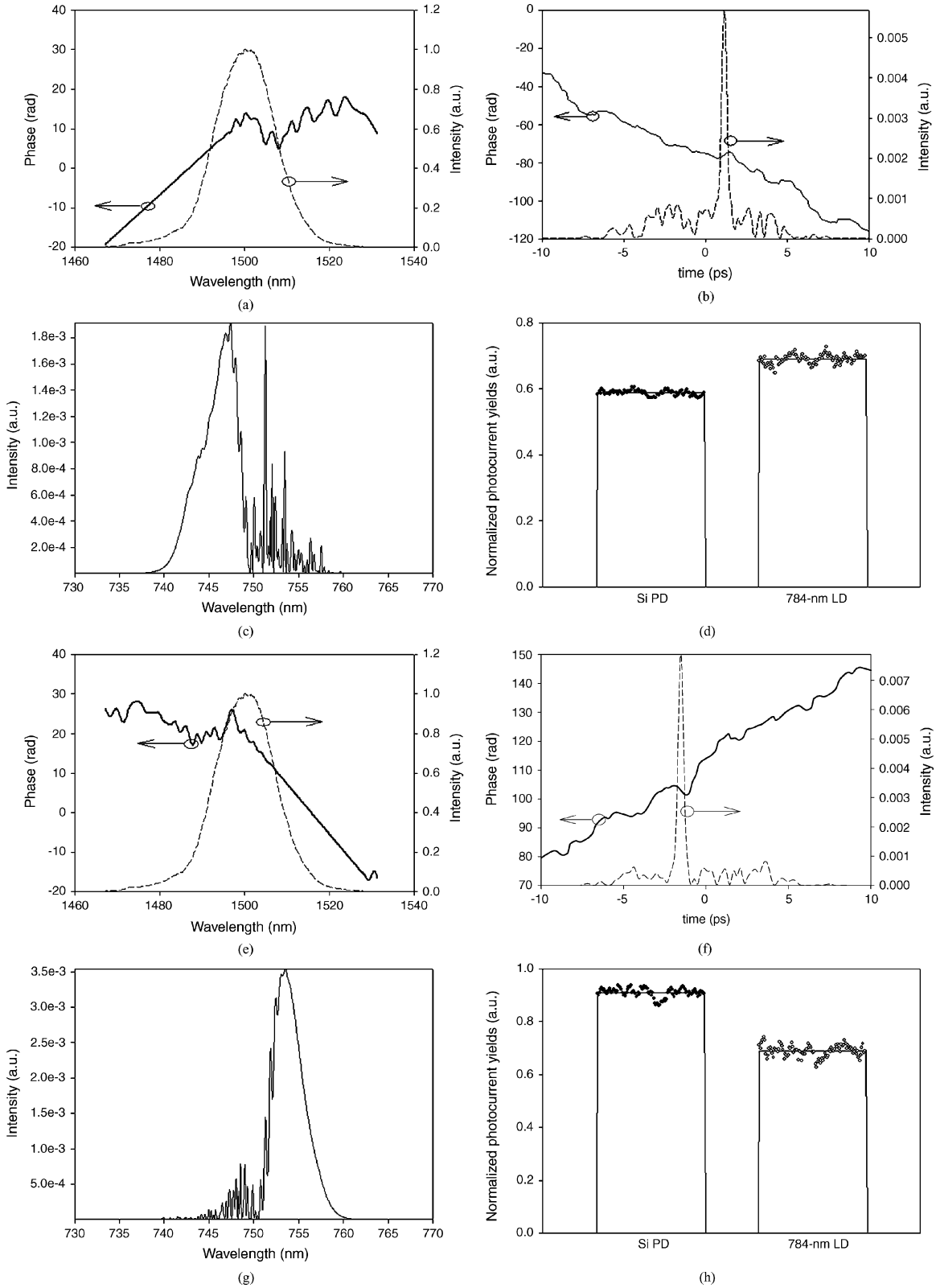


Fig. 5. Coherent control for (a)–(d) the ratio maximization and (e)–(h) the ratio minimization. (a), (e) Spectral phases (solid lines) that maximize and minimize the ratio of the LD yield in the TE case to the Si yield, respectively, together with the measured power spectrum (dashed lines). (b), (f) Calculated temporal phases (solid lines) and intensities (dashed lines) in ratio maximization and minimization cases, respectively. (c), (g) Calculated SH spectra in maximization and minimization cases, respectively. (d), (h) Measured photocurrents normalized by respective nonchirped case yields for the LD-silicon pair. Circles and solid lines represent measured and mean values, respectively.

from the 784-nm LD in the TE case to that from the Si PD. The measured power spectrum is also shown for the sake of clarity. Note that the region corresponding to wavelengths below 1500 nm exhibits linear wavelength dependence. This characteristic was observed every time we ran the algorithm, although the slope varied. This result agrees with the experiment based on dye materials, where it was explained using the simultaneous arrival of the corresponding frequency components [22]. The corresponding temporal intensity and phase were calculated as shown in Fig. 5(b). In order to verify the relationship between the spectral response and photocurrent yield, it is worthwhile to examine the spectral distribution of the SH spectrum. Fig. 5(c) shows the SH spectrum calculated using the power spectrum as well as the phase in Fig. 5(a). One can note that it leans toward the shorter wavelength region, where the spectral response of the LD overwhelms that of silicon in Fig. 3. Thus, the SH spectrum increases the photocurrent of the LD with respect to the Si PD. The bar graph in Fig. 5(d) illustrates the yield contrast when this phase was applied. Here, 100 dots and the top solid line represent measured and averaged photocurrents, respectively, for each diode, obtained by simultaneously reading the two lockin amplifiers. Note that the beam coupled into silicon was attenuated so that the yields from the two diodes were balanced in the nonchirped case. This graph indicates that the ratio approaches up to $\sim 1.20$. And the yield contrast is clear even with the input power fluctuation and noises. This is reasonably close to the calculated ratio, 1.40. The slight discrepancy might be caused by imperfect nonchirped case yield matching at 1500 nm or by nonideal phase manipulation in the LCM. Note that the maximum ratio obtained in a similar experiment using dye materials [22] was $\sim 1.3$. Also note that the contrast can be improved simply by using shorter pulses.

The converse case is illustrated in Fig. 5(e)–(h). The algorithm obtained the spectral phase in Fig. 5(d), which minimizes the normalized photocurrent ratio [calculated temporal intensity and phase are shown in Fig. 5(f)]. In contrast to the profile in Fig. 5(a), linear phase is observed for wavelengths above 1500 nm. The calculated SH spectrum also peaks in this region, as shown in Fig. 5(g). Since the TP spectrum of the LD is reduced for long wavelengths, the photocurrent ratio is minimized. Fig. 5(h) shows that now the ratio is reduced to $\sim 0.75$. The average optical powers were held at the same level as the previous case. Note that the LD yield was not changed very much but only the silicon yield increased by 55%, compared to Fig. 5(d). This is due to the higher peak intensity of the shaped pulse in Fig. 5(f) compared to that in 5(b). The measured ratio was in good agreement with the calculated value of 0.72. Note that in [22], this ratio minimization was not attempted.

## IV. TPA-Based Intensity AC Measurement

In this section we discuss the effect of the TPA spectral response on the TPA-based AC measurements. As mentioned in Section I, in order to achieve accurate pulsewidths, it is important to have a flat TPA spectral response, especially when measuring very short pulses. The effect of nonuniform TP spectral response depends on the pulse shape and may lead either to apparent pulse broadening or shortening in AC measurements. This phenomenon is analogous to the dependence of SHG-based pulse measurements to chirp in the case of limited phase-matching bandwidth [45].

With our TPA devices, AC measurement must be performed in the collinear geometry. Therefore, the resulting trace is subject to the background signal and interferometric fringes. In our experiment, therefore, we removed fringes by averaging dozens of traces and removed background signals in software. The remaining term is written as

$$G_2(\tau) = \int_{-\infty}^{\infty} H(\omega) \left| \int_{-\infty}^{\infty} e(t)e(t-\tau)\exp(-j\omega t)\,dt \right|^2 d\omega. \tag{3}$$

Note that when $H(\omega)$ is flat, (3) reduces to an ideal intensity AC function, i.e., $G_2(\tau) = \int I(t)I(t-\tau)dt$. Also, the zero-delay case coincides with (1). Knowing the latter fact, one can draw without difficulty a picture about the relationship between the TPA yield and the AC pulsewidth. Let us assume that a certain pulse shape gives a higher photocurrent yield in diode A than in diode B. Again, this corresponds to the AC intensity at $\tau = 0$. For small delays close to zero, the power spectrum of the cross term in (3), i.e., the integrand without $H(\omega)$, will not be changed significantly, and the yield will remain larger in diode A. If we assume that the two diodes have similar TPA photocurrents for higher delays, the AC pulsewidth measured in diode A will be shortened with respect to diode B.

To find the pulse shapes showing the pulsewidth discrepancy clearly, the evolutionary algorithm was used again. The merit function in this case involved the photocurrent differences between the two diodes at several selected delays. The spectral phase obtained in this way was applied to the pulse shaper and after passing the Michelson interferometer, the pulse was coupled into diodes. The optical power was adjusted so that no saturation could occur. TP-induced photocurrents were measured by a lockin amplifier while the delay was changed. Averaged and background free signals were normalized so that the zero-delay signal is unity. Each correlation trace was recorded ten times and then averaged together.

Two examples are included, with Fig. 6(a)–(c) and (d)–(f) corresponding to the cases where pulsewidths appear broader in the Si PD and in the 784-nm LD, respectively. Intensity AC traces measured and simulated for the pulse with phase and power spectrum in Fig. 6(a) are shown in (b) and (c), respectively (circles: Si PD; solid line: 784-nm LD). One can clearly see that the LD shortened the apparent pulsewidth. In this case the evolutionary algorithm found a trick such that the second side lobes are just above or below 0.5-amplitude for silicon and for the LD, respectively. This emphasizes the difference in FWHMs. The apparent AC FWHMs were 4.22 ps for silicon and 2.96 ps for the LD, resulting in 30% measurement discrepancy. The simulation result in Fig. 6(c) predicts 5.31- and 4.48-ps FWHMs for the silicon and LD traces, respectively, giving 16% discrepancy. Given the subtle differences between the silicon and LD traces, we believe the prediction is in reasonable qualitative agreement with the data. Using the formula in [49], we

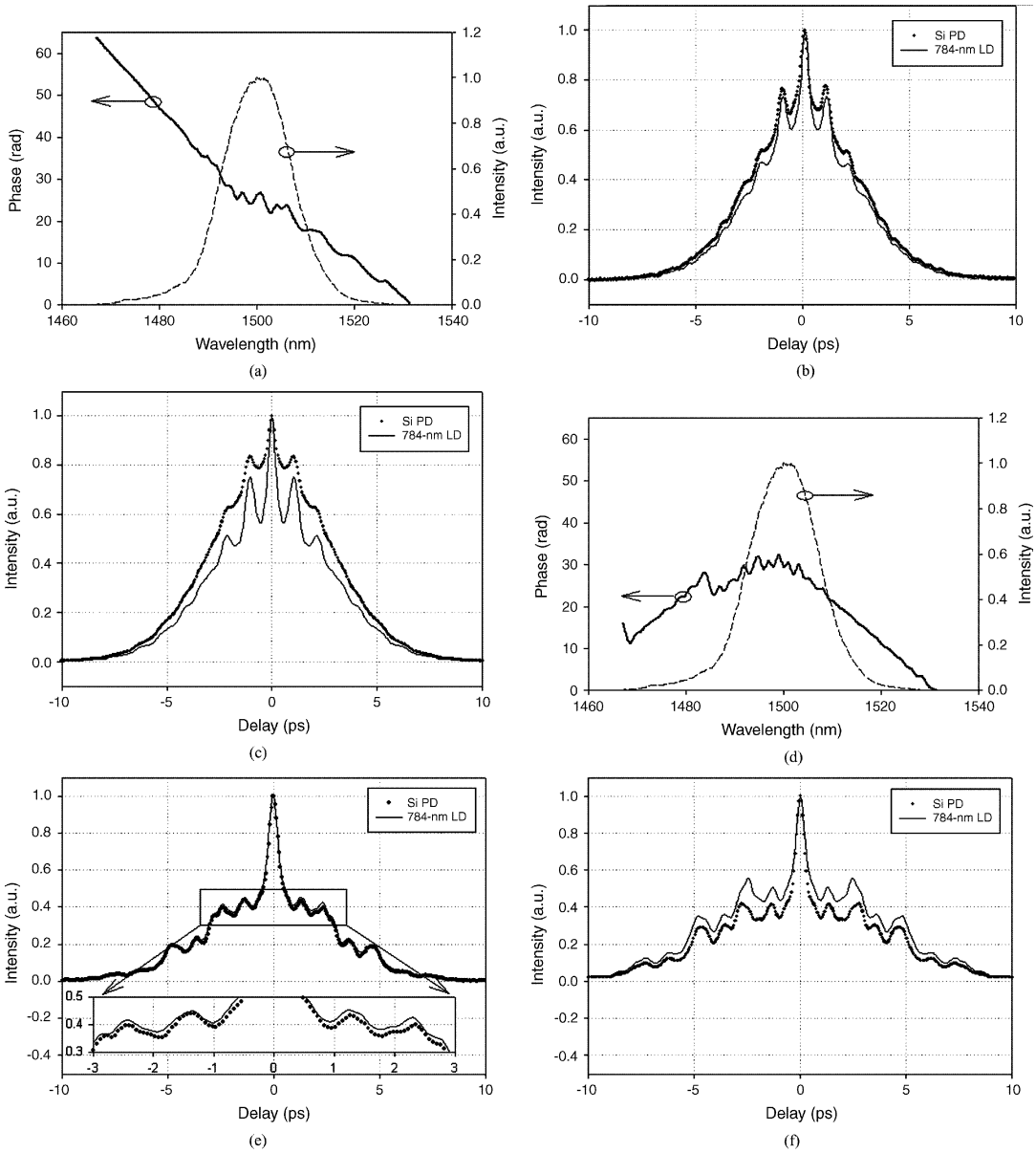


Fig. 6. (a)–(c): Pulsewidth contrast maximization for the shorter LD AC case. (a) The power spectrum and phase used for generating (b) measured and (c) simulated AC traces (circles: Si PD; solid line: 784-nm LD in the TE case). The LD AC has a shorter width. (d)–(f): Pulsewidth contrast maximization for the longer LD AC case. (d) The power spectrum and phase used for generating (e) measured and (f) simulated AC traces (circles: Si PD; solid line: 784-nm LD in the TE case). The inset in (e) magnifies the rectangular region. The width from the LD is longer than the Si PD.

have also extracted the rms pulsewidths of 3.43 ps for silicon and 3.33 ps for the LD, giving $\sim$100-fs difference. This value is close to the rms width of the original transform-limit pulse, i.e., $\sim$150 fs. The simulated rms widths were 3.59 ps for silicon and 3.32 ps for the LD. Now we have 270-fs discrepancy. The widths are listed in Table I for the sake of comparison.

The latter part of Fig. 6 shows the converse case. Now, the trace measured by the LD is broader than that for silicon. In the data this is best observed in the inset of Fig. 6(e). Some small asymmetric features are present due to imperfect averaging. AC FWHMs were 0.967 ps for the Si PD and 1.10 ps for the LD. Thus, the LD showed $\sim$14% broader width. In the simulation, the silicon and LD AC traces had FWHMs of 0.755 ps and 5.49 ps, respectively. This huge discrepancy was due to the side peak near 0.5-amplitude, as shown in Fig. 6(f). Therefore, comparison of rms widths is more useful. Root-mean-square pulsewidths were again extracted from the data using the formula in [49]: 3.98 ps for the Si PD and 4.07 ps for the LD.

TABLE I
MEASURED AND CALCULATED FWHM AND rms WIDTHS

| Case | Diode | FWHM (ps) | | RMS (ps) | |
|---|---|---|---|---|---|
| | | Measured | Calculated | Measured | Calculated |
| Fig. 6(a)–(c) | Si PD | 4.22 | 5.31 | 3.43 | 3.59 |
| | 784-nm LD | 2.96 | 4.48 | 3.33 | 3.32 |
| Fig. 6(d)–(f) | Si PD | 0.967 | 0.755 | 3.98 | 4.93 |
| | 784-nm LD | 1.10 | 5.49 | 4.07 | 5.20 |

Root-mean-square widths are larger than AC FWHMs, as one can expect from the shape of AC traces. Since this gives 86-fs discrepancy, the LD still introduces a significant pulsewidth error. The rms pulsewidths calculated from the simulation result were 4.93 ps for silicon and 5.20 ps for the LD, giving 265-fs discrepancy. These results consistently indicate that the AC trace from silicon is of shorter duration than that from the LD. The results are also listed in Table I. In these measurements the differences in pulsewidths estimated from the two different TP detectors are significantly greater than the variation observed when repeated measurements are performed with a single one of the TP detectors. The results clearly indicate that for certain semiconductor diodes, a nonflat spectral response has the potential to introduce distortions into TPA-based AC measurements. The degree of distortion depends on the pulse shape and is expected to become larger for shorter pulses with larger optical bandwidths.

## V. Conclusion

The research on coherent control that has been performed mainly for the understanding of matter-light interactions may open new possibilities for practical real-world applications. For this reason, coherent control in semiconductors is worth pursuing. In this paper we demonstrated, for the first time to our knowledge, the optimization of the ratio of photocurrent yields from two different semiconductor devices by coherently controlling their nonresonant TPA. The ratio swung from $\sim 0.75$ to $\sim 1.20$, which is limited by the input pulse bandwidth and the degree of difference in the TPA spectral responses. We also illustrated the relationship between the photocurrent ratio and SH spectrum peak. The capability to modulate the ratio of photocurrent yields in different diodes, according to pulse shape, has potential application to demultiplexer-free TPA-based detection of pulse shape-coded signals.

The yield contrast was due to distinct TPA spectral responses. A nonflat response behaves as a filtering function so that the TP-induced SH spectrum is spectrally modified, similar to the effect of the phase-matching function in SHG. When a semiconductor with nonflat TPA response is applied for pulsewidth measurements, it can potentially distort intensity AC traces. We observed that for certain pulse shapes, a laser diode TPA detector could introduce 14% broadening or 30% shortening, relative to the ideal intensity AC FWHMs. In measuring very short pulses, this pulsewidth modification imposed by the nonideal response will become more significant. The effects reported in this paper are expected to become stronger with broader source bandwidth or with semiconductor devices band-engineered for greater variation in TPA spectral response. However, even with $\sim 15$-nm bandwidth and with commercially available diodes, noticeable contrasts in yields and pulsewidths were observed in our experiment.

## References


[1] H. Rabitz, R. D. Vivie-Riedle, M. Motzkus, and K. Kompa, "Whither the future of controlling quantum phenomena," *Science*, vol. 288, pp. 824–828, May 2000.

[2] R. J. Gordon and S. A. Rice, "Active control of the dynamics of atoms and molecules," *Annu. Rev. Phys. Chem.*, vol. 48, pp. 601–641, 1997.

[3] A. P. Heberle, J. J. Baumberg, and K. Köhler, "Ultrafast coherent and destruction of excitons in quantum wells," *Phys. Rev. Lett.*, vol. 75, pp. 2598–2601, 1995.

[4] E. Dupont, P. B. Corkum, H. C. Liu, M. Buchanan, and Z. R. Wasilewski, "Phase-controlled currents in semiconductors," *Phys. Rev. Lett.*, vol. 74, pp. 3596–3599, 1995.

[5] A. M. Weiner, "Femtosecond pulse shaping using spatial light modulators," *Rev. Sci. Instrum.*, vol. 71, pp. 1929–1960, 2000.

[6] D. Meshulach and Y. Silberberg, "Coherent quantum control of multiphoton transitions by shaped ultrashort optical pulses," *Phys. Rev. A, Gen. Phys.*, vol. 60, pp. 1287–1292, 1999.

[7] A. Assion, T. Baumert, M. Bergt, T. Brixner, B. Kiefer, V. Seyfried, M. Strehle, and G. Gerber, "Control of chemical reactions by feedback-optimized phase-shaped femtosecond laser pulses," *Science*, vol. 282, pp. 919–922, 1998.

[8] R. J. Levis, G. M. Menkir, and H. Rabitz, "Selective bond dissociation and rearrangement with optimally tailored, strong-field laser pulses," *Science*, vol. 292, pp. 709–713, Apr. 2001.

[9] V. V. Lozovoy, I. Patirk, and M. Dantus, "Multiphoton intrapulse interference IV. Ultrashort laser pulse spectral phase characterization and compensation," *Opt. Lett.*, vol. 29, pp. 775–777, 2004.

[10] J. M. Dela Cruz, I. Pastirk, M. Comstock, V. V. Lozovoy, and M. Dantus, "Use of coherent control methods through scattering biological tissue to achieve functional imaging," *Proc. Nat. Acad. Sci.*, vol. 101, pp. 16996–17001, 2004.

[11] J. Erland, V. G. Lyssenko, and J. M. Hvam, "Optical coherent control in semiconductors: Fringe contrast and inhomogenous broadening," *Phys. Rev. B, Condens. Matter*, vol. 63, no. 155317, pp. 1–8, Apr. 2001.

[12] I. Brener, P. C. M. Planken, M. C. Nuss, M. S. C. Luo, S. L. Chuang, L. Pfeiffer, D. E. Leaird, and A. M. Weiner, "Coherent control of terahertz emission and carrier populations in semiconductor heterostructures," *J. Opt. Soc. Amer. B, Opt. Phys.*, vol. 11, pp. 2457–2469, 1994.

[13] J. M. Fraser, A. Haché, A. I. Shkrebtii, J. E. Sipe, and H. M. van Driel, "Three color coherent generation and control of current in low-temperature-grown GaAs," *Appl. Phys. Lett.*, vol. 74, pp. 2014–2016, 1999.

[14] N. Garro, S. P. Kennedy, A. P. Heberle, and R. T. Phillips, "Coherent control of two-photon transitions," *Phys. Stat. Sol. (b)*, vol. 221, pp. 385–389, 2000.

[15] Ü. Özgür, C.-W. Lee, and H. O. Everitt, "Control of coherent acoustic phonons in semiconductor quantum wells," *Phys. Rev. Lett.*, vol. 86, pp. 5604–5607, 2001.

[16] H. G. Breunig, T. Voss, I. Rückmann, and J. Gutowski, "Coherent control of biexcitonic polarization," *Phys. Rev. B, Condens. Matter*, vol. 66, no. 193302, pp. 1–3, Nov. 2002.

[17] J. Kunde, B. Baumann, S. Arlt, F. Morier-Genoud, U. Siegner, and U. Keller, "Optimization of adaptive feedback control for ultrafast semiconductor spectroscopy," *J. Opt. Soc. Amer. B, Opt. Phys.*, vol. 18, pp. 872–881, 2001.

[18] T. Flissikowski, A. Betke, I. A. Akimov, and F. Henneberger, "Two-photon coherent control of a single quantum dot," *Phys. Rev. Lett.*, vol. 92, no. 227401, pp. 1–4, Jun. 2004.

[19] U. Siegner, M. Haiml, J. Kunde, and U. Keller, "Adaptive pulse compression by two-photon absorption in semiconductors," *Opt. Lett.*, vol. 27, pp. 315–317, 2002.

[20] J. M. Fraser and H. M. van Driel, "Quantum interference control of free-carrier density in GaAs," *Phys. Rev. B, Condens. Matter*, vol. 68, no. 085208, pp. 1–14, Aug. 2003.

[21] R. Fanciulli, A. M. Weiner, M. M. Dignam, D. Meinhold, and K. Leo, "Coherent control of Bloch oscillations by means of optical pulse shaping," *Phys. Rev. B, Condens. Matter*, vol. 71, no. 153304, pp. 1–4, Apr. 2005.

[22] J. P. Ogilvie, K. J. Kubarych, A. Alexandrou, and M. Joffre, "Fourier transform measurement of two-photon excitation spectra: Applications to microscopy and optimal control," *Opt. Lett.*, vol. 30, pp. 911–913, 2005.

[23] K. Leo, "Coherent effects in semiconductor heterostructures," in *Handbook of Advanced Electronic and Photonic Materials and Devices*, vol. 2, Semiconductors, H. S. Nalwa, Ed. San Diego, CA: Academic, 2001.

[24] A. Shimizu, "Two-photon absorption in quantum-well structures near half the direct band gap," *Phys. Rev. B, Condens. Matter*, vol. 40, pp. 1403–1406, Jul. 1989.

[25] K. Fujii, A. Shimizu, J. Bergquist, and T. Sawada, "Electric-field-induced changes in the two-photon absorption spectrum of multiple-quantum-well structures," *Phys. Rev. Lett.*, vol. 65, pp. 1808–1811, Oct. 1990.

[26] H. K. Tsang, R. V. Penty, I. H. White, R. S. Grant, W. Sibbett, J. B. D. Soole, H. P. LeBlanc, N. C. Andreadakis, E. Colas, and M. S. Kim, "Polarization and field dependent two-photon absorption in GaAs/AlGaAs multiquantum well waveguides in the half-band gap spectral region," *Appl. Phys. Lett.*, vol. 59, pp. 3440–3442, Dec. 1991.
[27] T. H. Wood, C. A. Burrus, A. H. Gnauck, J. M. Wiesenfeld, D. A. B. Miller, D. S. Chemla, and T. C. Damen, "Wavelength-selective voltage-tunable photodetector made from multiple quantum wells," *Appl. Phys. Lett.*, vol. 47, pp. 190–192, 1985.
[28] A. Larsson, P. A. Andrekson, S. T. Eng, and A. Yariv, "Tunable superlattice p-i-n photodetectors: Characteristics, theory, and applications," *IEEE J. Quantum Electron.*, vol. 24, no. 5, pp. 787–801, May 1988.
[29] S. Goswami, P. Bhattacharya, and J. Singh, "Wavelength selective detection using excitonic resonances in multiquantum-well structures," *IEEE J. Quantum Electron.*, vol. 27, no. 4, pp. 875–877, Apr. 1991.
[30] K. W. Goossen, J. E. Cunningham, M. B. Santos, and W. Y. Jan, "Voltage-tunable multiple quantum well photodetector vertically integrated with voltage-tunable multiple quantum well filter," *Appl. Phys. Lett.*, vol. 62, pp. 3229–3231, 1993.
[31] S. Goswami, P. Bhattacharya, and J. Cowles, "Temporal response characteristics of a $In_{0.53}Ga_{0.47}As$/InP quantum well phototransistors," *IEEE Trans. Electron Devices*, vol. 40, no. 11, pp. 1970–1976, Nov. 1993.
[32] D. A. B. Miller, "Laser tuners and wavelength-sensitive detectors based on absorbers in standing waves," *IEEE J. Quantum Electron.*, vol. 30, no. 3, pp. 732–749, Mar. 1994.
[33] T. Coroy, R. M. Measures, T. H. Wood, and C. A. Burrus, "Active wavelength measurement system using an InGaAs-InP quantum-well electroabsorption filtering detector," *IEEE Photon. Technol. Lett.*, vol. 8, no. 12, pp. 1686–1688, Dec. 1996.
[34] S. Y. Hu, J. Ko, and L. A. Coldren, "Resonant-cavity InGaAs/InAl GaAs/InP photodetector arrays for wavelength demultiplexing applications," *Appl. Phys. Lett.*, vol. 70, pp. 2347–2349, May 1997.
[35] G. L. Christenson, A. T. T. D. Tran, Z. H. Zhu, Y. H. Lo, M. Hong, J. P. Mannaerts, and R. Bhat, "Long-wavelength resonant vertical-cavity LED/photodetector with a 75-nm tuning range," *IEEE Photon. Technol. Lett.*, vol. 9, no. 6, pp. 725–727, Jun. 1997.
[36] G. S. Li, W. Yuen, and C. J. Chang-Hasnain, "Wide and continuously tunable (30 nm) detector with uniform characteristics over tuning range," *Electron. Lett.*, vol. 33, pp. 1122–1124, Jun. 1997.
[37] X. Jiang, S. S. Li, and M. Z. Tidrow, "Investigation of a multistack voltage-tunable four-color quantum-well infrared photodetector for mid- and long-wavelength infrared detection," *IEEE J. Quantum Electron.*, vol. 35, no. 11, pp. 1685–1692, Nov. 1999.
[38] T. H. Shake, "Confidentiality performance of spectral-phase-encoded optical CDMA," *J. Lightw. Technol.*, vol. 23, no. 4, pp. 1652–1663, Apr. 2005.
[39] D. E. Leaird, Z. Jiang, and A. M. Weiner, "Experimental investigation of security issues in OCDMA: A code-switching scheme," *Electron. Lett.*, vol. 41, pp. 817–819, Jul. 2005.
[40] D. T. Reid, W. Sibbett, J. M. Dudley, L. P. Barry, B. Thomsen, and J. D. Harvey, "Commercial semiconductor devices for two photon absorption autocorrelation of ultrashort light pulses," *Appl. Opt.*, vol. 37, pp. 8142–8144, 1998.
[41] J. K. Ranka, A. L. Gaeta, A. Baltuska, M. S. Pshenichnikov, and D. A. Wiersma, "Autocorrelation measurement of 6-fs pulses based on the two-photon-induced photocurrent in a GaAsP photodiode," *Opt. Lett.*, vol. 22, pp. 1344–1346, 1997.
[42] L. P. Barry, B. C. Thomsen, J. M. Dudley, and J. D. Harvey, "Autocorrelation and ultrafast optical thresholding at 1.5 $\mu$m using a commercial InGaAsP 1.3 $\mu$m laser diode," *Electron. Lett.*, vol. 34, pp. 358–360, Feb. 1998.
[43] F. R. Laughton, J. H. Marsh, D. A. Barrow, and E. L. Portnoi, "The two-photon absorption semiconductor waveguide autocorrelator," *IEEE J. Quantum Electron.*, vol. 30, no. 3, pp. 838–845, Mar. 1994.
[44] Z. Zheng, A. M. Weiner, J. H. Marsh, and M. M. Karkhanehchi, "Ultrafast optical thresholding based on two-photon absorption GaAs waveguide photodetectors," *IEEE Photon. Technol. Lett.*, vol. 9, no. 4, pp. 493–495, Apr. 1997.
[45] A. M. Weiner, "Effect of group-velocity mismatch on the measurement of ultrashort optical pulses via 2nd harmonic-generation," *IEEE J. Quantum Electron.*, vol. 19, no. 8, pp. 1276–1283, Aug. 1983.
[46] Z. Zheng and A. M. Weiner, "Coherent control of second harmonic generation using spectrally phase coded femtosecond waveforms," *Chem. Phys.*, vol. 267, pp. 161–171, 2000.
[47] K. Naganuma, K. Mogi, and J. Yamada, "General method for ultrashort light pulse chirp measurement," *IEEE J. Quantum Electron.*, vol. 25, no. 6, pp. 1225–1233, Jun. 1989.
[48] G. Rudolph, "Evolution strategies," in *Evolutionary Computation 1: Basic Algorithms and Operators*, T. Bäck, D. B. Fogel, and T. Michalewicz, Eds., Bristol, U.K.: Institute of Physics, 2000, pp. 81–88.
[49] E. Sorokin, G. Tempea, and T. Brabec, "Measurement of the root-mean-square width and the root-mean-square chirp in ultrafast optics," *J. Opt. Soc. Amer. B, Opt. Phys.*, vol. 17, pp. 146–150, 2000.

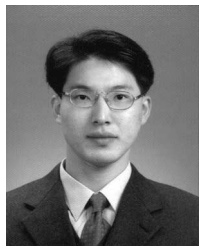

**Jung-Ho Chung** (S'01–M'06) was born in Jeonju, Korea, in 1971. He received the B.S. degree in electrical engineering from Seoul National University, Seoul, Korea, in 1997, and the M.S. and Ph.D. degrees from Purdue Unversity, West Lafayette, IN, in 2001 and 2005, respectively, both in electrical and computer engineering.

From 1993 to 1994, he served as a Private in the Korean Army. From 1997 to 1999, he was a Research Engineer at KTF, Seoul, Korea. In summer 2001, he was an Intern at Tycom, Eatontown, NJ. From 1999 to 2005, he was a Research Assistant at the Ultrafast Optics and Optical Fiber Communications Laboratory, Purdue University. He is now a Postdoctoral Researcher in the Optics and Quantum Electronics Group at the Research Laboratory of Electronics, Massachusetts Institute of Technology, Cambridge. He has researched ambiguities inherent in some pulse retrieval algorithms, space–time processing of femtosecond pulses, coherent control of two-photon absorption in semiconductors, and femtosecond pulse characterization using wavelength tunable optoelectronics. His current research interests include micromachining with femtosecond lasers, together with building laser systems for biomedical applications. He is the holder of four Korean patents.

Dr. Chung is a member of the IEEE Lasers and Electro-Optics Society (LEOS) and the Optical Society of America (OSA). He received the Student Travel Award from IEEE LEOS in May 2001, the Photonics Technology Access Program (PTAP) Grant from Optoelectronics Industry Development Association (OIDA) in June 2003, and the Graduate Student Fellowship from the IEEE LEOS in Oct. 2003.

**Andrew M. Weiner** (S'84–M'84–SM'91–F'95) received the Sc.D. degree in electrical engineering from the Massachusetts Institute of Technology (MIT), Cambridge, in 1984.

After graduation, he joined Bellcore, first as a Member of Technical Staff and later as Manager of Ultrafast Optics and Optical Signal Processing Research. In 1992, he moved to Purdue University, West Lafayette, IN, where he is currently the Scifres Distinguished Professor of Electrical and Computer Engineering. He has published five book chapters and over 175 journal articles. He has been author or coauthor of over 300 conference papers, including approximately 80 conference invited talks, and has presented over 70 additional invited seminars at university, industry, and government organizations. He is the holder of eight U.S. patents. His research focuses on ultrafast optical signal processing and high-speed optical communications. He is especially well known for pioneering the field of femtosecond pulse shaping, which enables generation of nearly arbitrary ultrafast optical waveforms according to user specification.

Prof. Weiner is a Fellow of the Optical Society of America. He has also served as Secretary/Treasurer of the IEEE Lasers and Electro-Optics Society (LEOS) and as a Vice-President of the International Commission on Optics (ICO). He has been the Co-Chair of the Conference on Lasers and Electro-optics and the International Conference on Ultrafast Phenomena, and has been an Associate Editor of several journals. He has also received numerous awards for his research.